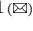


# PD-UniST: Prompt-Driven Universal Model for Unpaired H&E-to-IHC Stain Translation

Chujie Zhang<sup>1</sup>, Yangyang Xie<sup>2</sup>, Yinhao Li<sup>1</sup>, Xiao Liang<sup>2</sup>, Lanfen Lin<sup>3</sup>, and Yen-Wei Chen<sup>1</sup> 

<sup>1</sup> Graduate School of Information Science and Engineering, Ritsumeikan University, Japan

[chen@is.ritsumei.ac.jp](mailto:chen@is.ritsumei.ac.jp)

<sup>2</sup> Department of General Surgery, Sir Run-Run Shaw Hospital, Zhejiang University School of Medicine, China

<sup>3</sup> College of Computer Science and Technology, Zhejiang University, Hangzhou, China

**Abstract.** Virtual staining, which leverages generative artificial intelligence (AI) to produce immunohistochemistry (IHC)-stained tissue samples from hematoxylin and eosin (H&E)-stained images, has emerged as a cost-effective and accessible alternative to traditional IHC staining. Despite its potential, this approach faces three significant challenges: (1) the necessity of training a separate model for each tumor marker used in IHC staining, (2) the limited availability of large-scale datasets, and (3) the inherent diversity of staining patterns across different tissue types and markers. In this study, we address these challenges by introducing the **Prompt-Driven Universal** model for unpaired H&E-to-IHC Stain Translation (**PD-UniST**). Our approach incorporates two key innovations: (1) **Structure-Cognizant Organization Prompt Module (SCOPE)**, which employs textual prompts to guide region-specific generation, and (2) **Style-Prompt Unified Mapping Module (SPUME)**, which utilizes learnable prompts to capture task differences between various IHC stains and features a pathology-specific prompt-aware fusion layer for effective integration of visual features with task-specific prompts. Extensive experiments on two public datasets and one private dataset demonstrate that our method achieves state-of-the-art performance across five different translation tasks, significantly improving both structural preservation and staining pattern accuracy. In clinical evaluation, we further validate the effectiveness of our method through pathologists' assessment of both public and private datasets. The dataset and source code are available on anonymous GitHub at <https://github.com/chujie-zhang/PD-UniST>.

**Keywords:** Unpaired H&E-to-IHC stain translation · Prompt learning · Universal model.

## 1 Introduction

Hematoxylin and eosin (H&E) staining, a cost-effective technique for visualizing tissue structures, serves as pathologists' primary tool for initial histopathological

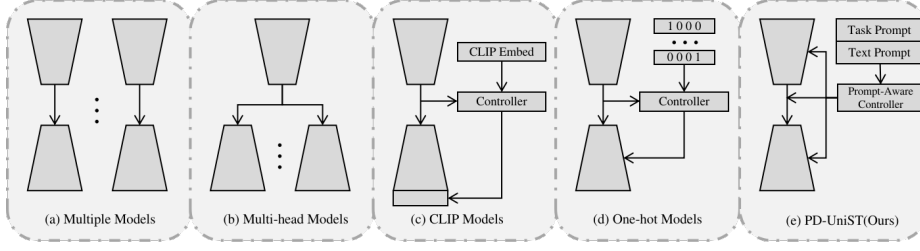


**Fig. 1.** It presents a comparative overview of five distinct architectural approaches in medical image translation frameworks: (a) Multiple Models utilizing separate translation networks, (b) Multi-head Models with one shared encoder and  $n$  task-specific decoders, (c) CLIP Models incorporating CLIP embeddings and a controller mechanism, (d) One-shot Models using a single network with binary code-guided controller, and (e) PD-UniST (our proposed method) which integrates task prompts and textual prompts with a prompt-aware controller.

analysis [18,17,11,19,8]. While immunohistochemistry (IHC) technology enables visualization of specific proteins through labeled antibodies [16,2], including tumor markers such as Ki67 (antigen Ki-67), HER2 (human epidermal growth factor receptor 2), ER (estrogen receptor), and PD-L1 (programmed death-ligand 1), its resource-intensive nature, including high costs, complex procedures, and tissue destruction, limits its clinical accessibility [9,10], particularly in resource-constrained settings.

Virtual staining, leveraging generative AI to create IHC-like images from H&E-stained samples, offers a cost-effective and accessible alternative to traditional IHC staining [15]. However, **this approach faces three key challenges:** (i) the need to train a model for each tumor marker used in IHC staining, as shown in Fig. 1(a), (ii) the limitation of small datasets due to the labor-intensive, time-consuming nature of IHC staining and its susceptibility to operator bias, and (iii) the diversity of staining patterns across different tumor markers. Different tumor markers in IHC staining show positive staining in distinct cellular locations based on their characteristics. For instance, tumor markers such as Ki67, ER, and PR display cell nuclear staining, while HER2 and PD-L1 demonstrate cell membrane staining. Models should consider these differences when generating images with various tumor markers.

Previous works address the first two challenges through three main strategies [12,1,6]: multi-head networks with shared encoders and task-specific decoders (Fig. 1(b)) [12], CLIP-driven universal models using text embeddings (Fig. 1(c)) [1], and dynamic convolution models with one-hot task encoding (Fig. 1(d)) [6]. However, these approaches have limitations: multi-head networks suffer from structural redundancy, CLIP models struggle with medical terminology comprehension (e.g., HER2, Ki67), and orthogonal one-hot vector encodings fail to capture inter-task relationships. Notably, none of these methods addresses the varying cellular localization patterns across different IHC tumor markers.

To address the limitations of existing strategies and overcome the third challenge of diverse staining patterns across tumor markers, such as cell nuclear staining for Ki67, ER, and PR versus cell membrane staining for HER2 and PD-L1. We introduce the **Prompt-Driven Universal** model for unpaired H&E-to-IHC Stain Translation (PD-UniST), as illustrated in Fig. 1(e). Our novel approach involves the implementation of a cutting-edge Prompt-Aware Controller to regulate the model’s output. The methodology consists of two key modules: (1) Structure-Cognizant Organization Prompt Module (SCOPE), which utilizes textual information such as ‘cell nucleus/cell membrane’ to guide the model’s focus on specific regions during generation based on different tumor markers’ characteristics, and (2) Style-Prompt Unified Mapping Module (SPUME), which features a Prompt-Aware Fusion Layer specifically designed for pathological images to effectively integrate visual features with task-specific prompts.

The main contributions are summarised as follows:

- We introduce the Prompt-Driven Universal Model (PD-UniST) as a pioneering universal translation model capable of transforming H&E-stained images into IHC-stained images. This novel approach aims to overcome the limitations of current methodologies by guiding the model to focus on different cellular locations based on various tumor marker characteristics through both learnable task prompts and textual prompts.
- We design the Structure-Cognizant Organization Prompt Module (SCOPE), which employs textual prompts to guide the model’s generation process.
- We develop the Style-Prompt Unified Mapping Module (SPUME), which employs a prompt-aware fusion layer and predefined task prompts to effectively constrain the model’s generation process.
- We present our private dataset (PD) as a new public dataset to support further research in virtual IHC staining. The experimental results demonstrate state-of-the-art performance across two public datasets and one private dataset when compared with traditional methods. Clinical evaluation conducted by pathologists on both public and private datasets validates the effectiveness of our method.

## 2 Method

### 2.1 Problem Definition

The universal H&E-to-IHC stain translation is defined as the training of a single model that learns from diverse medical datasets to perform various image translation tasks. Given a set of  $K$  datasets, each dataset  $\mathcal{D}_k = (x_k^i, y_k^i, m_k)_{i=1}^{N_k}$  consists of  $N_k$  data pairs, where  $(x_k^i, y_k^i) \in (\mathcal{X}_k \times \mathcal{Y}_k)$ , and  $m_k$  represents the imaging modality of  $\mathcal{D}_k$ .

### 2.2 Overview

The overall architecture of PD-UniST is illustrated in Fig. 2(a). Given an input image  $\mathcal{X} \in \mathbb{R}^{B \times C \times H \times W}$ , predefined learnable task prompts  $P_T \in \mathbb{R}^{K \times D}$ , and

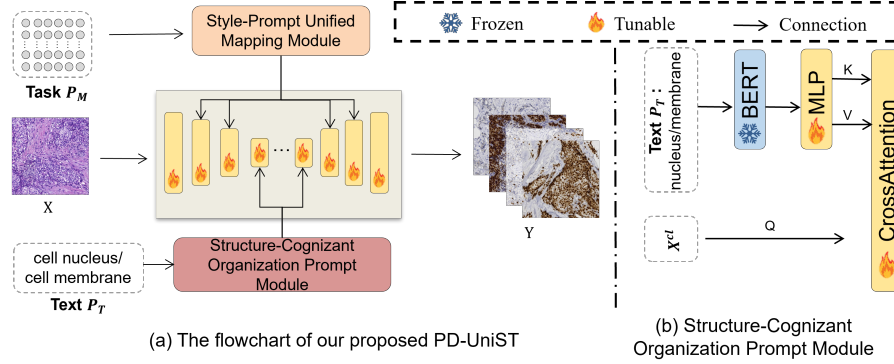


**Fig. 2.** Overall architecture of PD-UniST: (a) Pipeline showing the Style-Prompt Unified Mapping Module (SPUME) and Structure-Cognizant Organization Prompt Module (SCOPE) processing task prompts ( $P_M$ ) and text prompts ( $P_T$ ). (b) Detailed structure of SCOPE with frozen BERT, MLP, and cross-attention components. Note:  $X^{cl}$  represents the visual features of the current layer.

location-specific textual prompts  $P_M$  indicating either ‘cell nucleus’ or ‘cell membrane’ staining patterns, where  $K$  represents the number of tasks (IHC staining with different tumor markers) and  $D$  denotes the prompt dimension. Our framework encompasses five IHC staining tasks using the tumor markers HER2, ER, PR, Ki67, and PD-L1. As shown in Fig. 2(a), the input image  $\mathcal{X}$  enters the generator, while  $P_T$  and  $P_M$  are processed through the SCOPE and SPUME modules, respectively, integrating with visual features in the generator to guide image generation. By varying  $P_T$  and  $P_M$ , we can generate IHC-stained images with different tumor markers.

### 2.3 Structure-Cognizant Organization Prompt Module (SCOPE)

Immunohistochemical (IHC) staining reveals distinct subcellular localization patterns for different tumor markers. Specifically, biomarkers such as Ki67, ER, and PR exhibit cell nuclear staining patterns, while HER2 and PD-L1 show characteristic cell membrane staining. To effectively capture these location-specific staining characteristics, we propose the Structure-Cognizant Organization Prompt Module (SCOPE) framework, which integrates visual features with structured text priors (Fig. 2(b)) for pathology image translation.

Given an input image  $\mathcal{X} \in \mathbb{R}^{B \times C \times H \times W}$  and location-specific textual prompts  $P_T$  indicating either ‘cell nucleus’ or ‘cell membrane’ staining patterns, SCOPE processes the text information through a two-stage pipeline. First, a specialized biomedical BERT encoder [3], pretrained on biomedical domain knowledge, extracts contextual features from the textual prompts. These features are then refined through a learnable MLP projection layer and integrated with visual features via a cross-attention mechanism: **Output** =  $CrossAttention(MLP(BERT$



$(P_T)), \mathbf{X}^{cl})$ , where  $\mathbf{X}^{cl}$  represents the visual features extracted from the current layer. The framework is trained end-to-end, with the BERT encoder frozen to ensure stable text representations while allowing the multilayer perceptron (MLP) and cross-attention components to adapt to specific staining patterns.

## 2.4 Style-Prompt Unified Mapping Module (SPUME)

This section introduces the Style-Prompt Unified Mapping Module (SPUME), a novel framework that leverages the Prompt-Aware Fusion Layer (PAFL) for controlled IHC stain generation. Unlike conventional one-hot task encoding methods that treat each staining task independently, we hypothesize that inherent correlations exist among different IHC translation tasks. To capture these complex relationships, we propose integrating a task prior matrix within each PAFL, enabling dynamic interactions among diverse tasks.

The key innovation lies in the PAFL design, which centers on the prior fusion layers. For each layer, we initialize a task prior matrix  $\mathbf{P} \in \mathbb{R}^{K \times D}$ , where  $K$  represents the number of tasks and  $D$  denotes the prior dimension. Given the current layer’s visual features  $\mathbf{x}^{cl}$  and IHC ID  $t$ , we select the corresponding task-specific prior vector  $\mathbf{p}^t \in \mathbb{R}^{1 \times D}$  for feature enhancement. Our study encompasses five IHC staining tasks using the tumor markers HER2, ER, PR, Ki67, and PD-L1. The prior fusion layer implements a dual-stream architecture through the cross-attention module, each executing two key operations: 1) Prior Stream: Updates task prior vectors by learning from image features  $p_{i+1}^t = MLP(CrossAttention(LN(p_i^t), (x_i^{cl}))) + p_i^t$ . 2) Feature Stream: Refines features using updated task priors  $x_{i+1}^{cl} = MLP(CrossAttention(LN(x_i^{cl}), LN(p_{i+1}^t))) + x_i^{cl}$ , where  $LN$  denotes Layer Normalization.

## 2.5 Total Loss

The comprehensive loss function in our model comprises the basic GAN loss and the proposed loss terms. The total loss is formulated as:

$$l_{total} = \lambda_{adv}^D \times l_{adv}^D + \lambda_{adv}^G \times l_{adv}^G + \lambda_{cyc} \times l_{cyc} + \lambda_{idt} \times l_{idt} + \lambda_{PatchNCE} \times l_{PatchNCE} \quad (1)$$

Where  $l_{adv}^G$  and  $l_{adv}^D$  represent the adversarial losses,  $l_{cyc}$  represents the cycle-consistency loss,  $l_{idt}$  denotes the identity loss, and  $l_{PatchNCE}$  denotes the contrastive learning loss [13]. The coefficients  $\lambda_{adv}^D$ ,  $\lambda_{adv}^G$ ,  $\lambda_{cyc}$ ,  $\lambda_{idt}$ , and  $\lambda_{PatchNCE}$  are used to balance these loss terms.

# 3 Experiments

## 3.1 Experimental Setup

**Dataset.** We evaluate our method on three datasets: two public datasets and one private dataset from Sir Run-Run Shaw Hospital. The public datasets include: (1) the Breast Cancer Immunohistochemical (BCI) challenge dataset [7],

**Table 1.** Quantitative evaluation of our proposed PD-UniST method against state-of-the-art single-task and universal models using S-SSIM and FID metrics across six different stain translations: H&E-to-HER2 (MIST), H&E-to-ER (MIST), H&E-to-PR (MIST), H&E-to-Ki67 (MIST), H&E-to-HER2 (BCI), and H&E-to-PD-L1 (PD). The best results are highlighted in bold. Note: ‘SSIM’ in the table represents the structural component of SSIM (denoted as SSIM instead of S-SSIM for space efficiency). The term ‘single-task’ describes models limited to generating IHC staining for one specific tumor marker, whereas ‘multi-task’ refers to models capable of generating IHC staining for multiple different tumor markers.

Method	$MIST_{HER2}$		$MIST_{ER}$		$MIST_{PR}$		$MIST_{Ki67}$		$BCI_{HER2}$		$PD_{PDL1}$	
	SSIM	FID	SSIM	FID	SSIM	FID	SSIM	FID	SSIM	FID	SSIM	FID
<b>Single-task Models</b>												
CycleGAN[20]	0.21	240.3	0.54	125.7	0.41	96.1	0.54	343.9	0.56	83.5	0.51	142.7
[20] w/ SCOPE	0.53	110.6	0.57	83.9	0.55	74.6	0.59	91.1	0.58	75.6	0.54	125.3
MUNIT[4]	0.53	74.1	0.58	70.6	0.59	70.4	0.49	54.5	0.51	82.9	0.53	90.9
[4] w/ SCOPE	0.56	70.2	0.61	65.8	0.62	66.5	0.52	51.2	0.54	77.6	0.56	85.4
CUT[14]	0.63	66.8	0.68	43.7	0.63	54.6	0.67	76.1	0.59	65.0	0.61	84.1
[14] w/ SCOPE	0.64	62.3	0.69	41.5	0.65	53.9	0.67	71.4	0.62	64.3	0.62	82.2
ASP[5]	0.65	51.4	0.70	41.4	0.70	44.8	0.70	51.0	0.66	65.1	0.64	72.0
[5] w/ SCOPE	0.66	<b>50.8</b>	0.70	<b>40.1</b>	0.70	<b>42.9</b>	<b>0.71</b>	49.6	0.67	<b>63.9</b>	0.65	69.5
<b>Universal Models</b>												
VIMs(CLIP)[1]	0.65	156.8	0.61	132.4	0.63	115.7	0.64	98.6	0.60	142.5	0.64	138.9
One-hot[6]	0.65	142.1	0.65	73.3	0.62	65.7	0.64	55.4	0.63	92.2	0.66	85.6
PD-UniST	<b>0.68</b>	54.5	<b>0.70</b>	46.1	<b>0.70</b>	43.3	0.69	<b>49.6</b>	<b>0.68</b>	65.5	<b>0.68</b>	<b>68.3</b>

comprising 3,896 training and 977 testing image pairs, and (2) the Multi-IHC Stain Translation (MIST) dataset [5], containing approximately 4,000 training and 1,000 testing pairs for each of its four IHC stains (HER2, ER, Ki67, and PR). The Private Dataset (PD) uses the programmed death-ligand 1 (PD-L1) as the tumor marker, which consists of 3,600 training and 1,050 testing pairs with 21 patients. We collect sequential pathological tissues from the liver of 21 patients, which underwent H&E and IHC stain respectively. Since a single tissue can only be stained once, we utilized sequential tissues to create paired H&E and IHC stains, which explains why obtaining perfectly pixel-aligned H&E-IHC image pairs is physically impossible. For data preprocessing, we followed the same protocol as described in [7]. All images have a resolution of  $1024 \times 1024$  pixels.

**Implementation Details** We employ CycleGAN [20] as our baseline, maintaining identical architectures for both generator and discriminator. For training, we use a batch size of 1 and the Adam optimizer with  $\beta_1 = 0.5$  and  $\beta_2 = 0.999$ . The initial learning rate is set to  $2 \times 10^{-4}$ , which decays linearly to zero by the end of training. Detailed information is available in the anonymous GitHub.

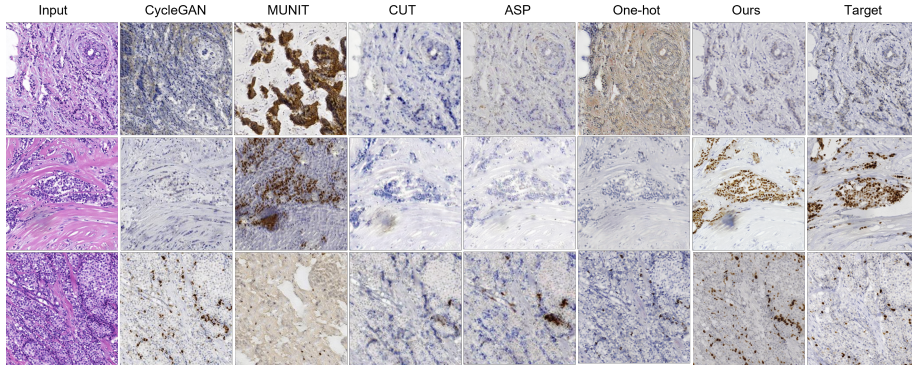


**Fig. 3.** Qualitative comparison of results across multiple biomarkers. Each row represents a different task (from top to bottom): H&E-to-HER2, H&E-to-PR, and H&E-to-Ki67. Note: Target domain examples are shown for reference and are selected based on shape similarity to the input.

**Table 2.** Ablation study of key modules (SPUME and SCOPE) on the MIST and PD datasets, evaluated using S-SSIM and FID metrics. The best results are shown in bold.

SPUME	SCOPE	MIST(H&E-to-Ki67)		PD(H&E-to-PDL1)	
		S-SSIM↑	FID↓	S-SSIM↑	FID↓
		0.54	343.9	0.51	142.7
✓		0.65	53.1	0.67	74.9
✓	✓	<b>0.69</b>	<b>49.6</b>	<b>0.68</b>	<b>68.3</b>

**Metrics.** The performance is evaluated using four metrics: Fréchet Inception Distance (FID), Structural component of Structural Similarity Index (S-SSIM), and two downstream task metrics (Accuracy (ACC) and Area Under the Curve (AUC)). Specifically, S-SSIM calculates only the structural component of SSIM between the input and generated images, defined as:  $S-SSIM(x, y) = \frac{\sigma_{xy} + c}{\sigma_x \sigma_y + c}$ .

**Compared methods.** We categorize the comparison methods into two types: single-task models, and universal models. Specifically, the single-task models include CycleGAN [20], CUT [14], ASP [5], and MUNIT [4]. The universal models encompass VIMs (CLIP) [1], and One-hot [6].

### 3.2 Experimental Results and Analysis

**Quantitative Comparison** Quantitative evaluation demonstrates the effectiveness of the PD-UniST method. As shown in Tab. 1, PD-UniST achieves competitive or superior performance compared to both single-task and universal models. In the universal models category, PD-UniST consistently outperforms

**Table 3.** Clinical evaluation results on the MIST and PD datasets, evaluated using ACC and AUC metrics. The best results are shown in bold.

SPUME	SCOPE	MIST(H&E-to-Ki67)		PD(H&E-to-PDL1)	
		ACC↑	AUC↑	ACC↑	AUC↑
		0.65	0.75	0.64	0.71
✓		0.68	0.78	0.66	0.73
✓	✓	<b>0.70</b>	<b>0.79</b>	<b>0.69</b>	<b>0.77</b>

VIMs(CLIP) and One-hot methods, achieving higher SSIM and lower FID scores across different staining translations. ASP w/SCOPE gets better FID scores in single-task settings because its contrastive learning and focused attention creates more realistic textures when optimized for specific stains. This specialization better matches the patterns of individual markers. In contrast, our PD-UniST learns shared features across all six datasets, building stronger structural understanding but with slightly weaker modeling for individual datasets.

**Qualitative Comparison** The qualitative comparison in Fig. 3 demonstrates the results across multiple staining translation tasks. The results of VIMs (CLIP) [1] are not shown due to their inferior performance. Through comparison with various methods and target images, our approach achieves both accurate staining patterns and precise tissue morphology preservation, closely matching the target IHC expressions.

**Ablation Study** Our ablation study in Tabs. 2 and 3 demonstrates the complementary benefits of the SPUME and SCOPE components. The baseline model achieves moderate performance, while adding SPUME substantially improves both structural similarity and image quality.

**Clinical Evaluation** To validate the clinical relevance of our method, we conducted a comprehensive evaluation involving an expert pathologist. For each method being evaluated, the pathologist assessed two sets of images: 50 pairs of method-generated H&E-to-IHC translations and 50 pairs of ground truth H&E-IHC images. The assessment involved classifying IHC expression levels into three categories: low, moderate, and high expression. As demonstrated in Tab. 3, by comparing the pathologist’s assessments of generated images against the ground truth using accuracy and AUC metrics, our method demonstrates substantial improvements in IHC expression level prediction. The enhanced performance across both metrics validates the clinical utility of our approach in accurately representing IHC expression patterns.

## 4 Conclusion

We present PD-UniST, a prompt-driven universal model for H&E-to-IHC stain translation featuring SCOPE for textual prompts and SPUME for task prompts. Through extensive experiments on public and private datasets, our approach demonstrates superior performance in quantitative, qualitative, and clinical evaluations, advancing virtual staining technology for clinical pathology applications.

**Acknowledgments.** This work was supported in part by JST SPRING, Japan Grant Number JPMJSP2101 and the Grant in Aid for Scientific Research from the Japanese Ministry for Education, Science, Culture and Sports (MEXT) under the Grant Nos. 20KK0234, 21H03470, and 20K21821, and in part by the National Key Research and Development Project (No. 2022YFC2504605).

**Disclosure of Interests.** The authors have no competing interests to declare that are relevant to the content of this article.

## References

1. Dubey, S., Chong, Y., Knudsen, B., Elhabian, S.Y.: Vims: virtual immunohistochemistry multiplex staining via text-to-stain diffusion trained on uniplex stains. In: International Workshop on Machine Learning in Medical Imaging. pp. 143–155. Springer (2024)
2. Fedchenko, N., Reifenrath, J.: Different approaches for interpretation and reporting of immunohistochemistry analysis results in the bone tissue—a review. *Diagnostic pathology* **9**, 1–12 (2014)
3. Gu, Y., Tinn, R., Cheng, H., Lucas, M., Usuyama, N., Liu, X., Naumann, T., Gao, J., Poon, H.: Domain-specific language model pretraining for biomedical natural language processing (2020)
4. Huang, X., Liu, M.Y., Belongie, S., Kautz, J.: Multimodal unsupervised image-to-image translation. In: Proceedings of the European conference on computer vision (ECCV). pp. 172–189 (2018)
5. Li, F., Hu, Z., Chen, W., Kak, A.: Adaptive supervised patchnce loss for learning h&e-to-ihc stain translation with inconsistent groundtruth image pairs. In: International Conference on Medical Image Computing and Computer-Assisted Intervention. pp. 632–641. Springer (2023)
6. Lin, Y., Zeng, B., Wang, Y., Chen, Y., Fang, Z., Zhang, J., Ji, X., Wang, H., Zhang, Y.: Unpaired multi-domain stain transfer for kidney histopathological images. In: Proceedings of the AAAI Conference on Artificial Intelligence. vol. 36, pp. 1630–1637 (2022)
7. Liu, S., Zhu, C., Xu, F., Jia, X., Shi, Z., Jin, M.: Bci: Breast cancer immunohistochemical image generation through pyramid pix2pix. In: Proceedings of the IEEE/CVF conference on computer vision and pattern recognition. pp. 1815–1824 (2022)
8. Liu, S., Li, X., Zheng, A., Yang, F., Liu, Y., Guan, T., He, Y.: The generation of virtual immunohistochemical staining images based on an improved cycle-gan. In: Machine Learning and Intelligent Communications: 5th International Conference, MLICOM 2020, Shenzhen, China, September 26–27, 2020, Proceedings 5. pp. 137–147. Springer (2021)

9. Liu, S., Zhang, B., Liu, Y., Han, A., Shi, H., Guan, T., He, Y.: Unpaired stain transfer using pathology-consistent constrained generative adversarial networks. *IEEE transactions on medical imaging* **40**(8), 1977–1989 (2021)
10. Liu, Y., Li, X., Zheng, A., Zhu, X., Liu, S., Hu, M., Luo, Q., Liao, H., Liu, M., He, Y., et al.: Predict ki-67 positive cells in h&e-stained images using deep learning independently from ihc-stained images. *Frontiers in Molecular Biosciences* **7**, 183 (2020)
11. Miller, Q., Saeed, O., Mesa, H.: Clinical, pathologic, and molecular-genetic aspects of colorectal polyps. *Gastrointestinal Endoscopy Clinics* **32**(2), 313–328 (2022)
12. Ounissi, M., Sarbout, I., Hugot, J.P., Martinez-Vinson, C., Berrebi, D., Racoceanu, D.: Scalable, trustworthy generative model for virtual multi-staining from h&e whole slide images. *arXiv preprint arXiv:2407.00098* (2024)
13. Park, T., Efros, A.A., Zhang, R., Zhu, J.Y.: Contrastive learning for unpaired image-to-image translation. In: *Computer Vision–ECCV 2020: 16th European Conference, Glasgow, UK, August 23–28, 2020, Proceedings, Part IX* 16. pp. 319–345. Springer (2020)
14. Park, T., Efros, A.A., Zhang, R., Zhu, J.Y.: Contrastive learning for unpaired image-to-image translation. In: *Computer Vision–ECCV 2020: 16th European Conference, Glasgow, UK, August 23–28, 2020, Proceedings, Part IX* 16. pp. 319–345. Springer (2020)
15. Pati, P., Karkampouna, S., Bonollo, F., Comp  rat, E., Radi  , M., Spahn, M., Martinelli, A., Wartenberg, M., Kruithof-de Julio, M., Rapsomaniki, M.: Accelerating histopathology workflows with generative ai-based virtually multiplexed tumour profiling. *Nature Machine Intelligence* **6**(9), 1077–1093 (2024)
16. Ramos-Vara, J.A.: Technical aspects of immunohistochemistry. *Veterinary pathology* **42**(4), 405–426 (2005)
17. Sheikh, R.A., Min, B.H., Yasmeen, S., Teplitz, R., Tesluk, H., Ruebner, B.H., Tobi, M., Hatfield, J., Fligiel, S., Lawson, M.J.: Correlation of ki-67, p53, and adnab-9 immunohistochemical staining and ploidy with clinical and histopathologic features of severely dysplastic colorectal adenomas. *Digestive diseases and sciences* **48**, 223–229 (2003)
18. Soares, C.T., Frederigue-Junior, U., de Luca, L.A.: Anatomopathological analysis of sentinel and nonsentinel lymph nodes in breast cancer: hematoxylin-eosin versus immunohistochemistry. *International journal of surgical pathology* **15**(4) (2007)
19. Sousa, W.A.T.d., Rodrigues, L.V., Silva Jr, R.G.d., Vieira, F.L.: Immunohistochemical evaluation of p53 and ki-67 proteins in colorectal adenomas. *Arquivos de gastroenterologia* **49**, 35–40 (2012)
20. Xiao, Z., Kreis, K., Vahdat, A.: Tackling the generative learning trilemma with denoising diffusion gans. *arXiv preprint arXiv:2112.07804* (2021)